The Supplemetary materials include:

In supplementary Material 1, titled with "Forward modelling of the strong motion waveforms from one of the largest aftershocks (2008/05/13, 07h07)", we describe the details that the velocity models used in our inversion (Table 1) are able to adequately model the wave propagation in the area.

In supplementary Material 2, another largest aftershock ((2008/05/13, 07h07, Mw5.9) was further modelled using the same method as in supplementary Material 1, which is a further confirmation to the point that the velocity models used in the inversion are able to adequately model the wave propagation in the area.

In supplementary Material 3, we describe the details about the epicentre Determination of the 2008 Wenchuan mainshock.

Supplementary figure file include all the figures needed by the three suppllementary materials and two figures about the waveforms fitting from two inversion schemes, the optimal inversion and the inversion test delayer rupture not fully allowed (see more details in the main text).

http://dx.doi.org/10.1029/2012gl052516

Supplementary Material 1 : Forward modelling of the strong motion waveforms from one of the largest aftershocks (2008/05/13, 07h07)

We present here the waveform modelling of one of the largest aftershocks (2008/05/13, 07h07) which occurred close to the epicentral region of the main shock. The epicenter is located at (30.95°N, 103.24°E). We check with this approach that the velocity models of Table 1 are able to adequately model the wave propagation in the area. A further confirmation is given with another aftershock in the Supplementary material 2.

Because of the signal-to-noise ratio, we only use the strong motion stations relatively close to the event (see Figure S1). 8 of them are located in the mountain range (triangles with red contours) and 2 of them are located in the Sichuan Basin (triangles with green contours). The waveforms at the latter stations are modelled with an upper sedimentary layer, which is not used for the stations in the mountain range, according to the velocity model of Table 1.

We use an approach based on the direct waveform simulation with the discrete wavenumber method (Bouchon, 1981): we consider that the aftershock can be assimilated to a point source, and optimize, by an inverse technique (Neighborhood Algorithm ; Sambridge (1999)), its values of depth, strike, dip, rake, and magnitude, based on the waveform agreement in the frequency range [0.04Hz - 0.1Hz]. The optimal model is (depth, strike, dip, rake, Mw) = (9km, 229°, 52°, 126°, 5.7), in good agreement with the Global CMT (http://www.globalcmt.org) values (14km, 213°, 42°, 109°, 5.8). In Figure S2, we show the waveform agreement at the stations. The global misfit (0.28) shows that the waveforms are adequately modelled up to 0.1Hz. When using the velocity models of Table 1 to model the main shock waveforms, we are therefore confident that their complexities will be explained by realistic source properties, and not by propagation artefacts.

Supplementary Material 2 : Forward modelling of the strong motion waveforms from one of the largest aftershocks (2008/05/25, 08h21)

We present here the waveform modelling of one of the largest aftershocks (2008/05/25, 08h21) which occurred close to the rupture termination of the main shock. The epicenter is located at (32.52°N, 105.32°E). We check with this approach that the velocity models of Table 1 are able to adequately model the wave propagation in the area. This is a further confirmation of the analysis made in the Supplementary material 1, where the aftershock was located close to the epicenter of the main shock.

Because of the signal-to-noise ratio, we only use the strong motion stations relatively close to the event (see Figure S3). 3 of them are located in the mountain range (triangles with red contours) and 2 of them are located in the Sichuan Basin (triangles with green contours). The waveforms at the latter stations are modelled with an upper sedimentary layer, which is not used for the stations in the mountain range, according to the velocity model of Table 1.

We use an inverse approach based on the direct waveform simulation with the discrete wavenumber method (Bouchon, 1981): we consider that the aftershock can be assimilated to a point-source, and optimize, by an inverse technique (Neighborhood Algorithm ; Sambridge (1999)), its values of depth, strike, dip, rake, and magnitude, based on the waveform agreement in the frequency range [0.04Hz - 0.1Hz]. The optimal model is (depth, strike, dip, rake, Mw) = (18km, 65°, 83°, 186°, 5.9), in good agreement with the Global CMT (http://www.globalcmt.org) values (27km, 59°, 84°, 178°, 6.1). In Figure S4, we show the waveform agreement at the stations. The global misfit (0.29) shows that the waveforms are adequately modelled up to 0.1Hz. Together with similar results shown in the Supplementary material 1, this analysis shows that the velocity

models of Table 1 allows us to simulate adequate waveforms in the area.

Supplementary Material 3: Epicentre Determination of the 2008 Wenchuan mainshock

We present here the measurements of the polarization of the initial P waves, at strong motion stations close to the epicenter (Figure S5). We follow the general ideas presented by Alessandrini et al. (1994) (and references therein) or Scherbaum and Johnson (1990). For this analysis, we consider the 4s time window following the arrival of the P waves and determine the back-azimuth based on the ratio between North and East components in the frequency range [0.2Hz - 0.7 Hz]. We show in Figure S5 that the ray directions converge to a small area (see inset), close to the point 31.06°N, 103.4°E. This determination is useful to add a further constraint on the epicenter location, which is known to be a sensitive parameter in the kinematic source inversions. It also confirms that the horizontal components of the strong motion stations are adequately orientated.

References :

Alessandrini B., M. Cattaneo, M. Demartin, M. Gasperini, and V. Lanza (1994), A simple P-wave polarization analysis: its application to earthquake location, Annali di Geofisica, 38, 883-897

Bouchon, M. (1981), A simple method to calculate Green's functions for elastic layered media, Bull. Seism. Soc. Am., 71, 959-971.

Sambridge, M. (1999), Geophysical inversion with a neighbourhood algorithm. I. Searching a parameter space, Geophys. J. Int., 138, 479–494.

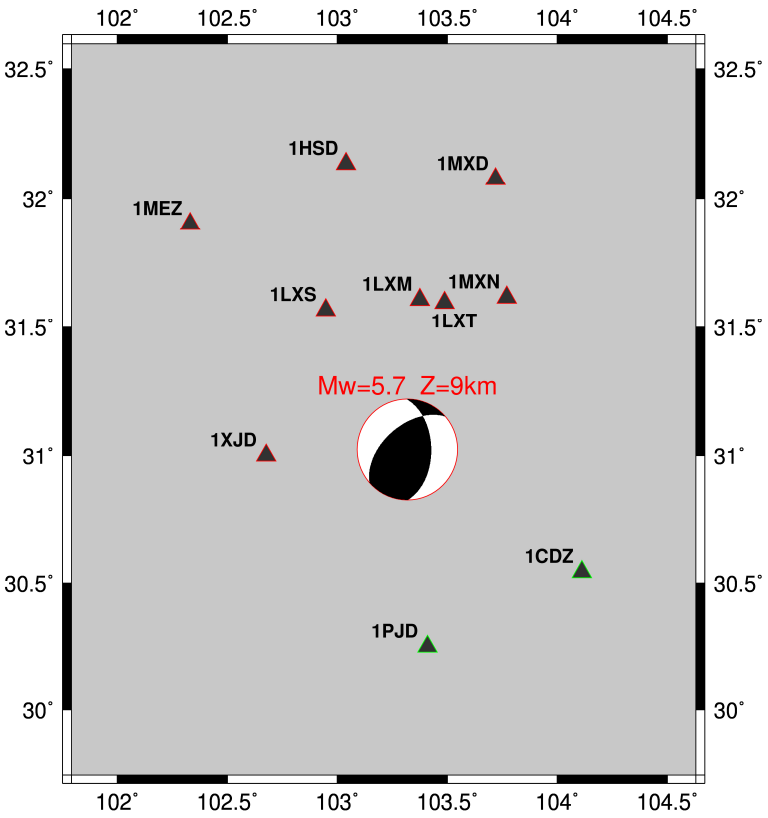

Figure S1: Map of the stations used to analyze the 2008/05/13 (07h07) aftershock. Stations with green contours are in the Sichuan Basin, and stations with red contours are in the mountain range. The optimal focal mechanism, magnitude and depth are shown.

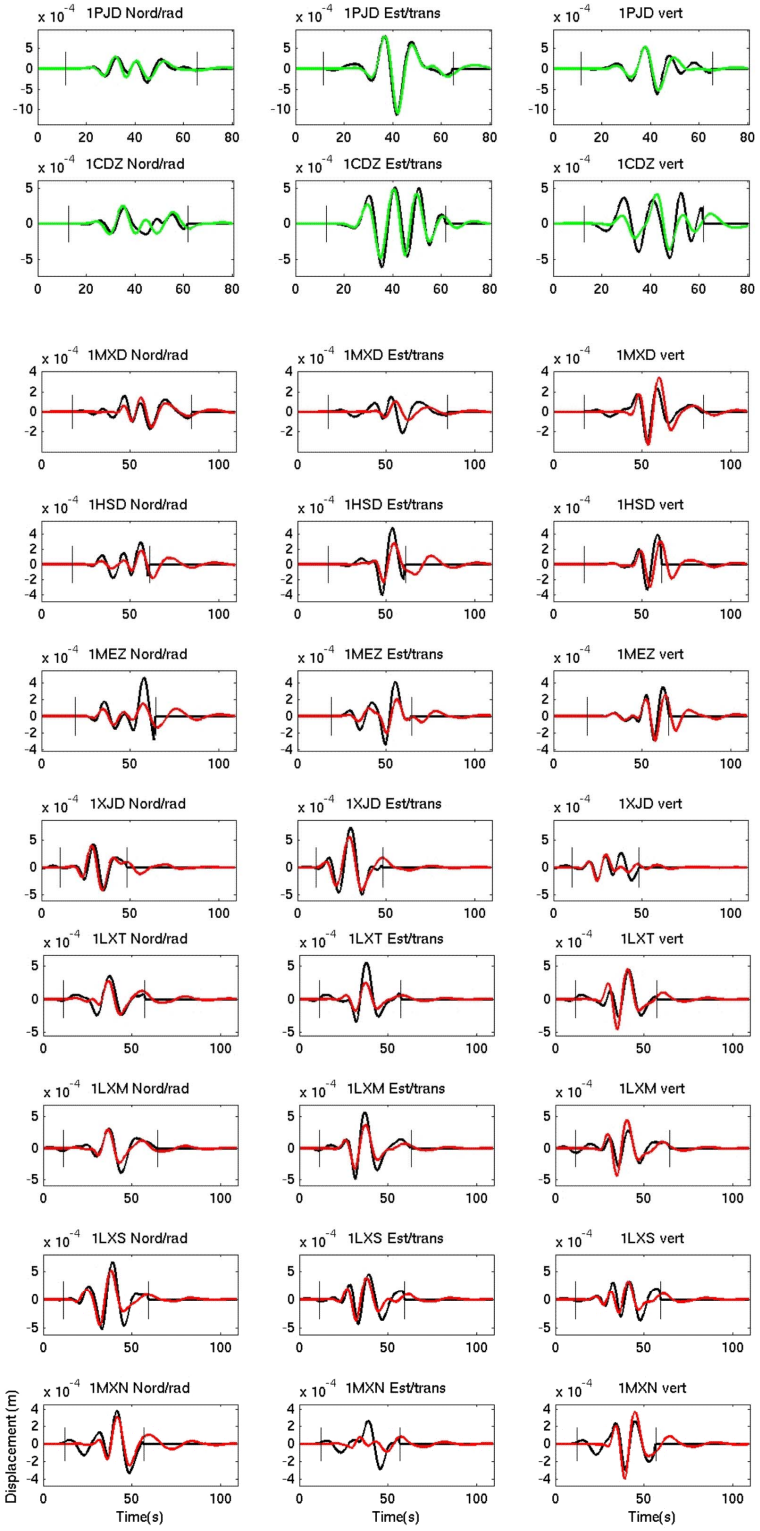

Figure S2: Agreement between data (black) and synthetics corresponding to the optimal model, in the [0.04Hz - 0.1Hz] frequency range. Synthetics are green when the stations are located in the

Sichuan Basin and red when located in the mountain range. The reference time corresponds to the aftershock origin time.

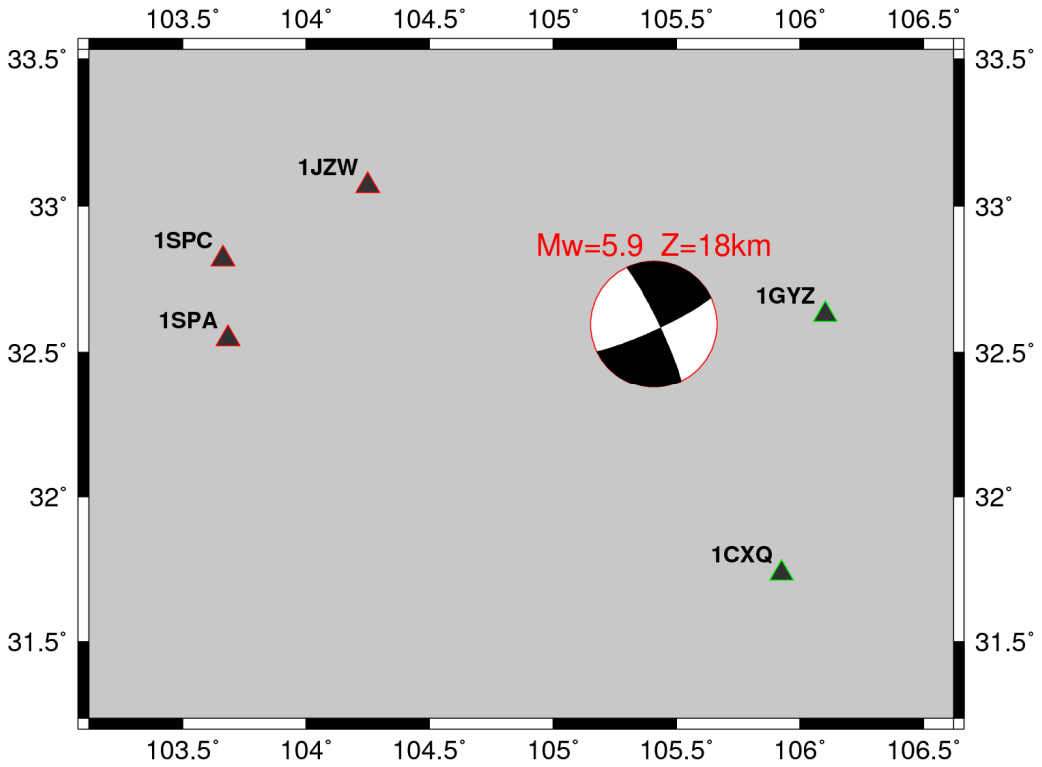

Figure S3: Map of the stations used to analyse the 2008/05/13 (07h07) aftershock. Stations with green contours are in the Sichuan Basin, and stations with red contours are in the mountain range. The optimal focal mechanism, magnitude and depth are shown.

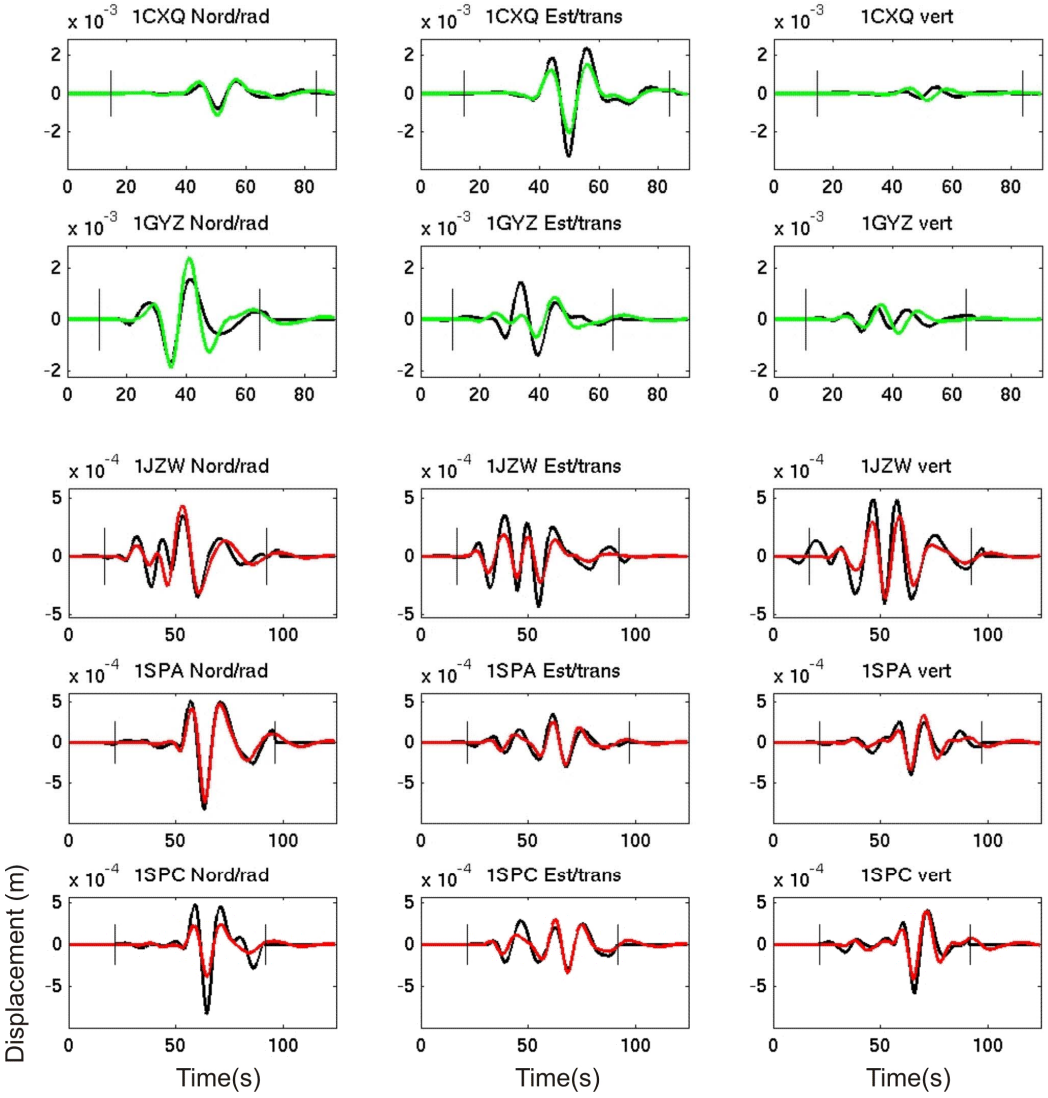

Figure S4: Agreement between data (black) and synthetics corresponding to the optimal model, in the [0.04Hz - 0.1Hz] frequency range. Synthetics are green when the stations are located in the Sichuan Basin and red when located in the mountain range. The reference time corresponds to the aftershock origin time.

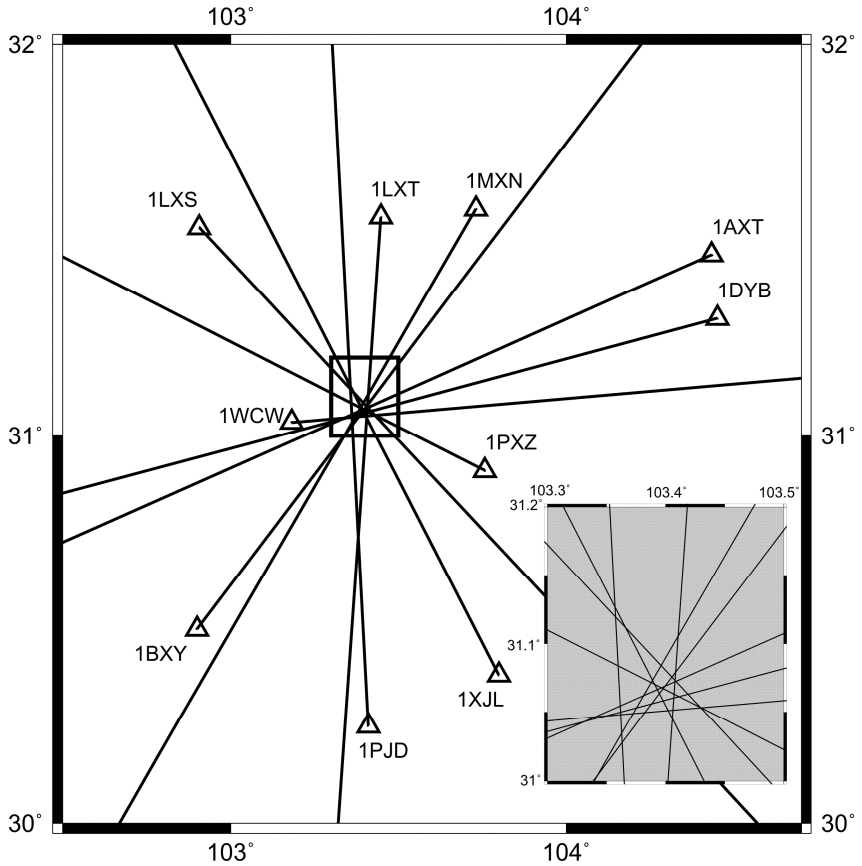

Figure S5: Epicenter location by polarization analysis of the initial P waves. Stations used in this analysis are indicated by triangles. The measured back-azimuths are shown by the straight lines starting from the station locations. The inset is a zoom of the square (thick lines) of the main figure. It can be seen that the rays define an epicentral region with an error of less than 5-7km.

The optimal fitting waveforms for all the components used in inversion

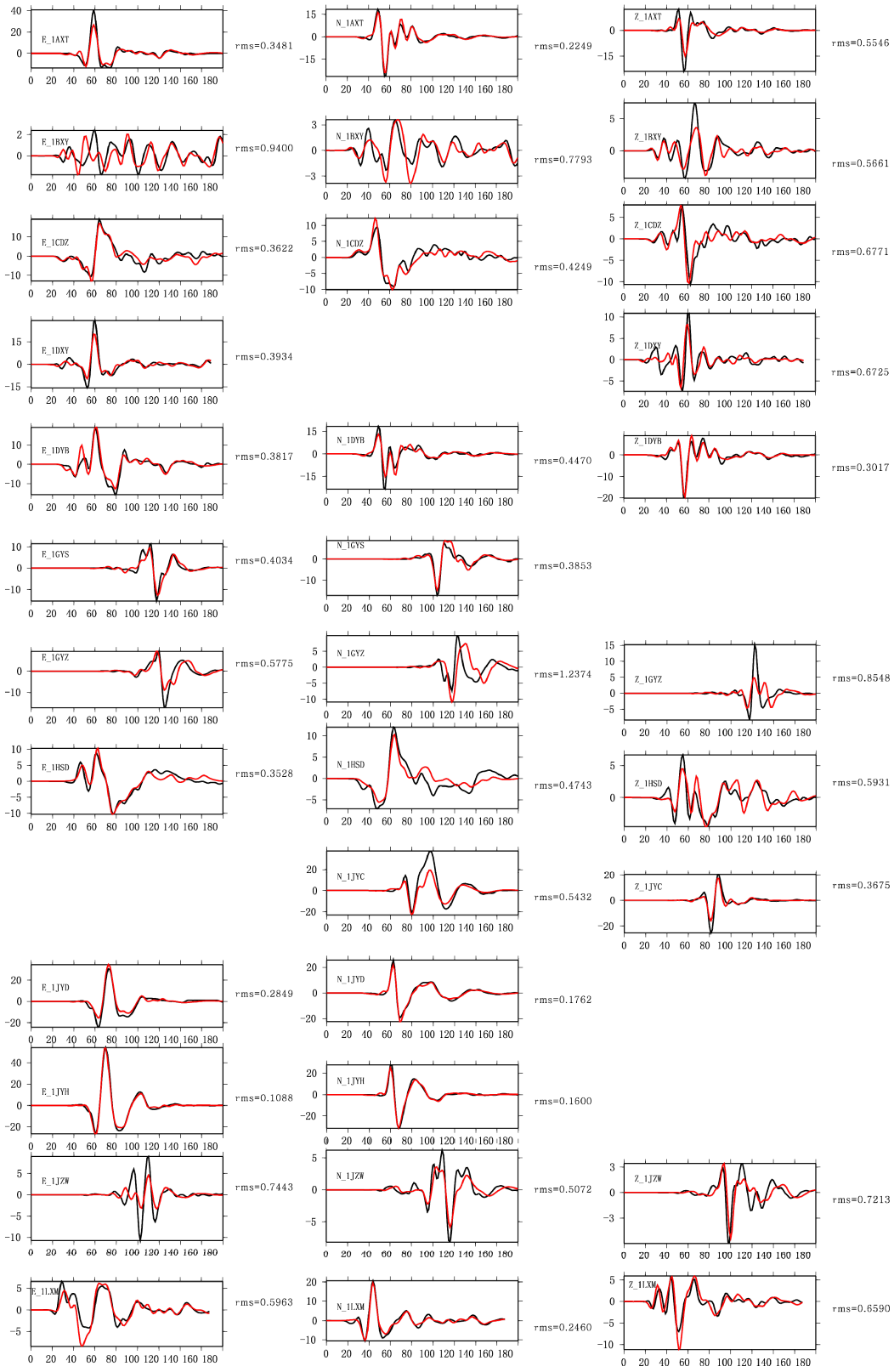

The optimal fitting waveforms for all the components used in inversion

Continued

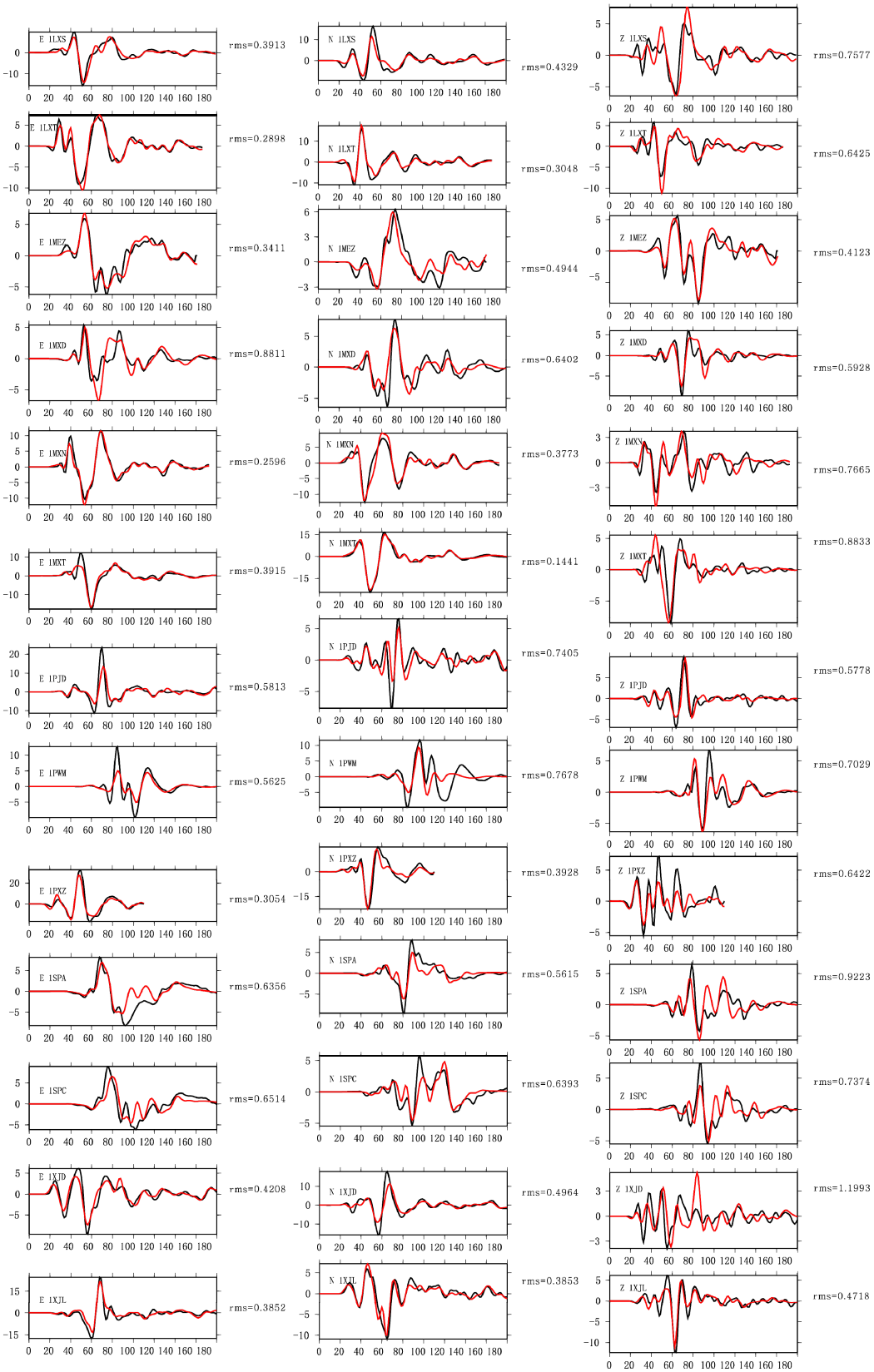

Figure S6: Agreement between observed and synthetic waveforms corresponding to the optimal model. All the 72 components from 26 stations used in our inversion are presented. The black and red lines are the observations and the predicted waveforms from the optimal inversion, respectively. The rms values for each component are shown to the right side and the total rms is 0.42.

The inversion test fitting waveforms for all the components

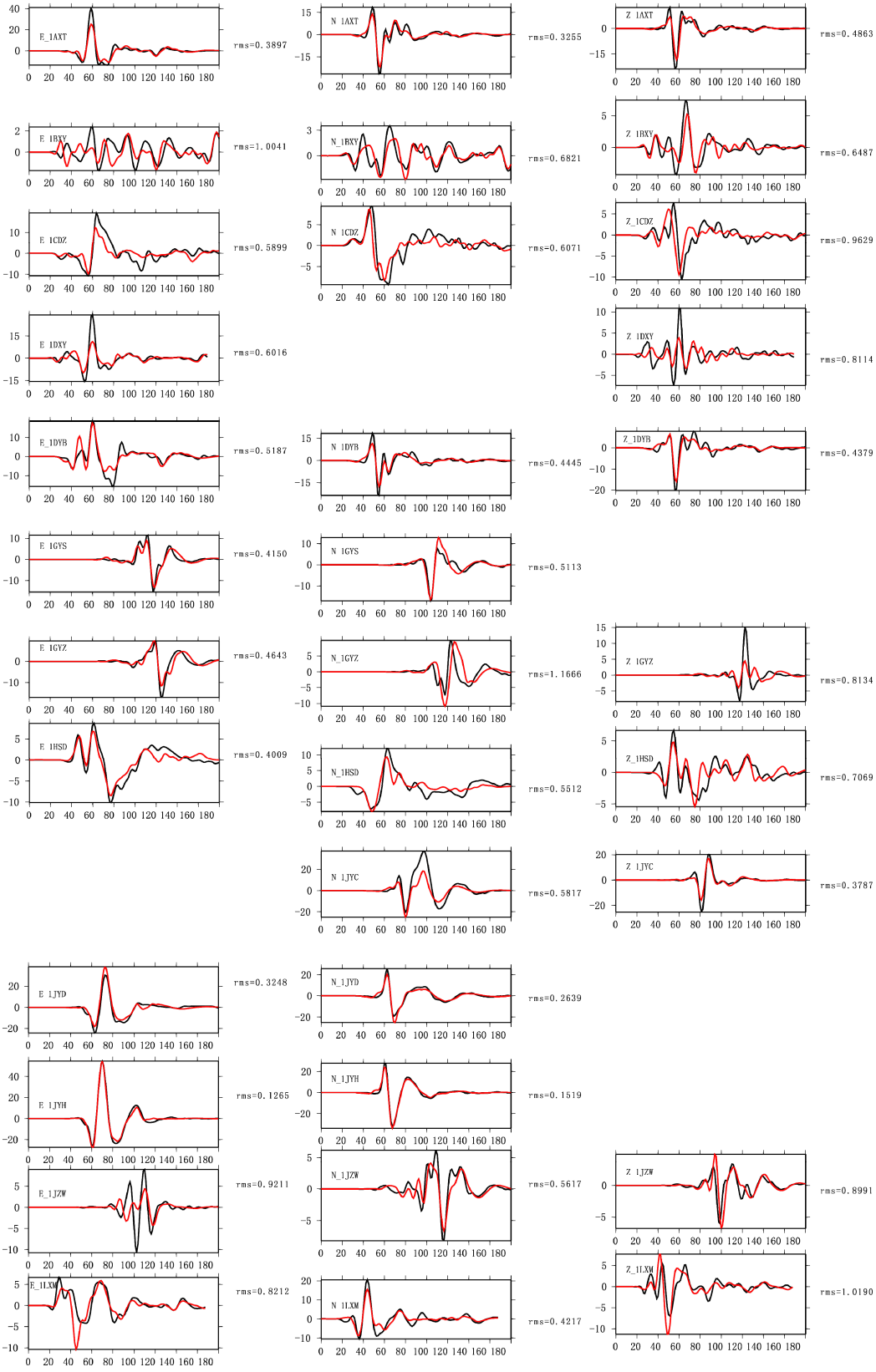

The inversion test fitting waveforms for all the components

Continued

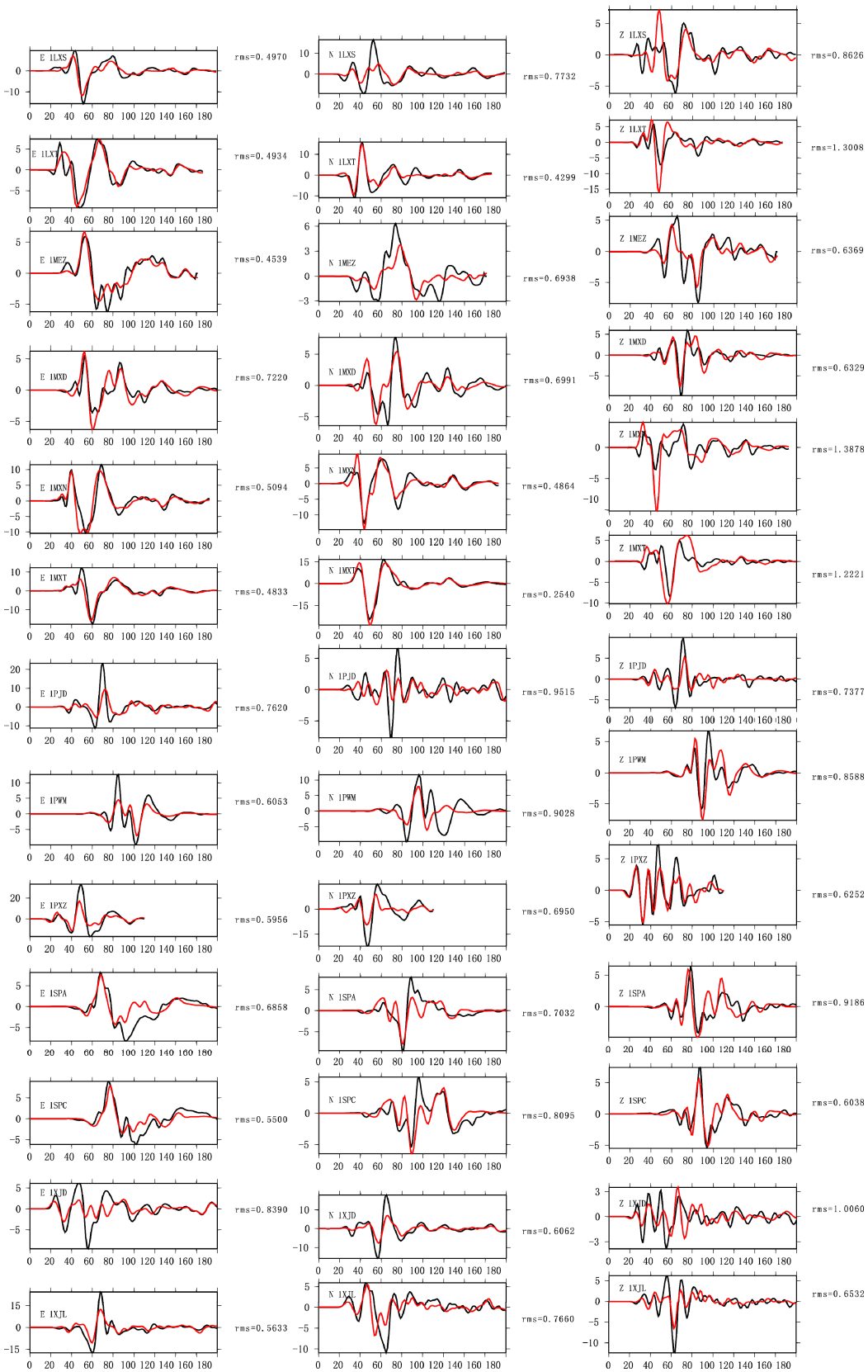

Figure S7: Agreement between observed and synthetic waveforms corresponding to the model where rupture delay is not fully allowed (hereafter referred as “inversion test”) . All the 72 components from 26 stations used in the inversion test are presented. The black and red lines are the observations and the predicted waveforms from the inversion test, respectively. The rms values for each component are shown to the right side. The total rms value increases moderately to 0.54, but the observed waveforms close to the main slip patch are clearly less well modeled compared to the optimal inversion. Please see more detailed discussion in the main text.